

Bidirectional Semi-supervised Dual-branch CNN for Robust 3D Reconstruction of Stereo Endoscopic Images via Adaptive Cross and Parallel Supervisions

Hongkuan Shi, Zhiwei Wang, Ying Zhou, Dun Li, Xin Yang, *Member, IEEE*, Qiang Li, *Member, IEEE*,

Abstract—Semi-supervised learning via teacher-student network can train a model effectively on a few labeled samples. It enables a student model to distill knowledge from the teacher's predictions of extra unlabeled data. However, such knowledge flow is typically unidirectional, having the performance vulnerable to the quality of teacher model. In this paper, we seek to robust 3D reconstruction of stereo endoscopic images by proposing a novel fashion of *bidirectional* learning between two learners, each of which can play both roles of teacher and student concurrently. Specifically, we introduce two self-supervisions, i.e., *Adaptive Cross Supervision* (ACS) and *Adaptive Parallel Supervision* (APS), to learn a dual-branch convolutional neural network. The two branches predict two different disparity probability distributions for the same position, and output their expectations as disparity values. The learned knowledge flows across branches along two directions: a cross direction (disparity guides distribution in ACS) and a parallel direction (disparity guides disparity in APS). Moreover, each branch also learns confidences to dynamically refine its provided supervisions. In ACS, the predicted disparity is softened into a unimodal distribution, and the lower the confidence, the smoother the distribution. In APS, the incorrect predictions are suppressed by lowering the weights of those with low confidence. With the adaptive bidirectional learning, the two branches enjoy well-tuned supervisions from each other, and eventually converge on a consistent and more accurate disparity estimation. The extensive and comprehensive experimental results on three public datasets demonstrate our superior performance over the fully-supervised and semi-supervised state-of-the-arts with a decrease of averaged disparity error by 13.95% and 3.90% at least, respectively.

Index Terms—Semi-supervised learning, Stereo matching, Endoscopic images

This work was supported in part by National Key R&D Program of China (Grant No. 2022YFE0200600), Fundamental Research Funds for the Central Universities (2021XXJS033), Research grants from United Imaging Healthcare Inc.

Hongkuan Shi, Zhiwei Wang, Ying Zhou, Qiang Li are with Britton Chance Center for Biomedical Photonics, Wuhan National Laboratory for Optoelectronics, Huazhong University of Science and Technology, Wuhan, 430074, China. Hongkuan Shi and Zhiwei Wang are the co-first authors. Qiang Li is the corresponding author. (email:liqiang8@hust.edu.cn)

Dun Li is with United Imaging Surgical Healthcare Co., Ltd. 99 Gaokeyuan Rd., Wuhan, 430074, China.

Xin Yang is with School of Electronic Information and Communications, Huazhong University of Science and Technology, Wuhan, 430074, China.

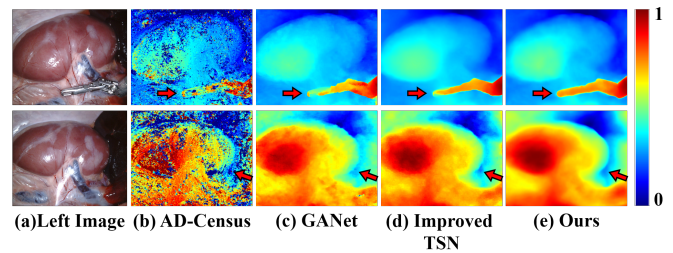


Fig. 1. Two examples of disparity estimation by different methods. (a) Left input image, (b-e) normalized disparity map predicted by traditional method AD-Census [3], fully-supervised method GANet [4], Improved TSN [5], and our method. The red arrows emphasize some challenging regions, e.g., organ edges and surgical instruments, where our method achieves visually better results.

I. INTRODUCTION

IN robot assisted minimally invasive surgery (RA-MIS), 3D reconstruction of the stereo-endoscopic scenes is an enabling step for preoperative model registration, intra-operative surgical planning and so on [1], [2]. An accurate and dense stereo-endoscopic 3D reconstruction is a must for a reliable RA-MIS, but extremely challenging because of the surgical scenes' low-textured appearance, occlusions and especially scarce labels due to *in-vivo* environments.

3D reconstruction of stereo images requires recovering a depth map by finding pixel matching relations along the horizontal epipolar line in a rectified left-right image pair. The depth is in inverse proportion to the disparity, and the latter is defined as a pixel's shifting distance from the left image to its corresponding position in the right image. Traditional methods [3], [6], [7] typically rely on intensity similarities for matching pixels. Thus, low-textured surfaces in endoscopic scenes could make most traditional methods fail, yielding incorrect sparse disparity maps as evidenced in Figure 1 (b).

Recently, the methods based on Convolutional Neural Network (CNN) have shown their impressive 3D reconstruction performance in both medical [5], [8]–[13] and non-medical [4], [14]–[20] domains. Depending on the label dependency, these methods can be categorized into *fully-supervised*, *self-supervised*, and *semi-supervised* approaches. Fully-supervised methods [4], [14] usually have an outstanding performance, but this comes with a price of laborious annotation of collected

samples (i.e., the ground-truth (GT) disparity maps). For the stereo-endoscopic images, the GT map is hard or even infeasible to acquire, especially for some *in-vivo* scenes. A CNN-based method trained on insufficient labeled samples usually suffers from an overfitting problem, which degrades its performance consequently. For example, Figure 1 (c) shows the results predicted by a recent fully-supervised method, i.e., GANet [4], trained on only 25 available labeled stereo endoscopic images.

The self-supervised methods [15]–[17] learn stereo disparity estimation models with no labeled samples. They first estimate a disparity map aligned with the left image, and then reconstruct a synthesized left image by warping the right image along the epipolar line according to the estimated disparities. Therefore, the learning objective is to minimize pixel-wise reconstruction loss between the real and synthesized left images. However, such pixel-wise loss is unreliable because of the inconsistent brightness, which is caused by a strong non-Lambertian reflection on the organ surfaces.

The semi-supervised methods [5], [11]–[13], [18]–[20] combine the strengths of both fully-supervised and self-supervised learnings. The supervised learning guarantees a more accurate disparity estimation by explicit guidance of GT maps, and the self-supervised learning enhances the generalization by distilling knowledge from the unlabeled samples. Among them, Teacher Student Network (TSN) based semi-supervised methods [12], [13], [19] have made great progress. In TSN, a teacher model is first trained in a supervised manner, and then predicts pseudo labels for unlabeled samples. A student model thus can be trained utilizing both labeled and unlabeled samples for further improving its performance. However, TSN often faces a dilemma when it comes to the medical data, e.g., endoscopic scenes, that is, the supervised teacher model hardly predicts highly confident pseudo labels due to few labeled data available for training, and teaches out a worse student model consequently.

In our previous work [5], we have improved TSN to address the above issue by introducing a semi-supervised teacher model to predict mostly correct pseudo labels, and a confidence network to further suppress the unreliable predictions with low confidence. Therefore, a more accurate student model can be trained by use of more reliable pseudo labels. Despite our success, the improved TSN still has limitations, for example, the teacher model has to be separately trained beforehand, and the knowledge flow is unidirectional from the teacher to student. Thus, the teacher’s performance becomes decisive, and its stagnant learning quality limits the possibility of a further improvement of the student’s performance.

In this paper, we break through the limitations, and propose a unified framework where the teacher-student and confidence networks can be trained jointly in a bidirectional semi-supervised fashion. As shown in the top of Figure 2, the unified framework is essentially a dual-branch CNN. Each branch utilizes a disparity estimation network (*DEnet*) and a confidence network (*Confnet*) to predict three maps of disparity probability distribution, disparity value, and confidence. The value map is an expectation of the distribution map.

In the fully-supervised learning, each branch is trained sepa-

ately on labeled samples, to predict their disparity value maps and corresponding confidence maps. In the self-supervised learning, *Adaptive Cross Supervision* (ACS) and *Adaptive Parallel supervision* (APS) are introduced to have the two branches mutually guide each other by taking the opposite’s predictions as supervisions. Specifically, ACS constrains each branch to predict a unimodal probability distribution with its peak aligned with the other’s disparity value, and meanwhile APS minimizes the L1 distance between the disparity values in the two branches. Moreover, the confidence adaptively controls each branch’s contribution to the learning of the other branch, and enhances the reliability of provided supervisions. That is, a lower confidence indicates a lower and wider peak of the unimodal distribution in ACS, and a less contribution of the supervision by a re-weighting strategy in APS, and vice versa.

In summary, our main contributions are listed:

- 1) We surmount the limitations of our previous improved TSN [5], and develop a novel semi-supervised dual-branch CNN for disparity estimation of stereo-endoscopic images. The two branches can mutually guide each other in a fashion of bidirectional learning, and eventually converge on a consistent and more accurate disparity estimation (see Figure 1 (d)–(e)).
- 2) We introduce ACS and APS as two kinds of the bidirectional supervisions, where the knowledge of each branch can be adaptively refined and flow along both cross and parallel directions to guide the learning of the other branch. The resulting well-tuned bidirectional supervisions maximize the efficacy of unlabeled data in the learning of our proposed dual-branch CNN.
- 3) The extensive and comprehensive experimental results on three public datasets demonstrate the effectiveness of two proposed bidirectional supervisions, and a superior performance of our method over the fully-supervised and semi-supervised state-of-the-arts with a decrease of average disparity error by 13.95% and 3.90% at least, respectively.

II. METHOD

In this section, we first introduce the architecture of dual-branch CNN in Sec. II-A, and then detail the self-supervised learning via APS and ACS in Sec. II-B, and the fully-supervised learning of each individual branch in Sec. II-C, and give implementation and training details in Sec. II-D.

A. Architecture of Dual-branch Network

1) *Dual-Branch Architecture*: The top part of Figure 2 illustrates the dual-branch CNN, and each branch consists of two key networks, i.e., a Disparity Estimation network (i.e., *DEnet*) and a Confidence network (i.e., *Confnet*). For clarity, we use two subscripts *a* and *b* to distinguish the networks and predictions in different branches, and the capital letters *A* and *B* to distinguish the two branches.

Given a pair of rectified left-right images (I_l, I_r) with the size of $H \times W$, Branch A predicts three maps of disparity probability distribution, disparity value, and confidence, which are denoted as P_a , D_a , and K_a , respectively. Also, Branch B predicts P_b , D_b , and K_b , simultaneously.

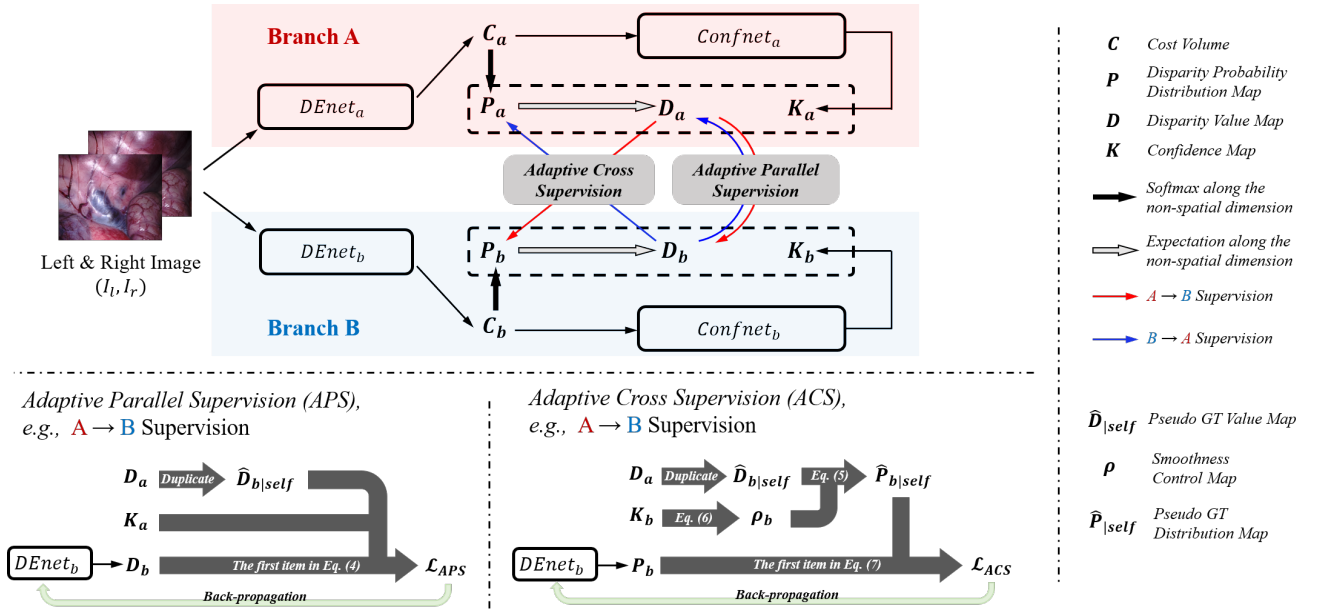


Fig. 2. Illustration of dual-branch CNN's architecture and its self-supervised learning by the two adaptive bidirectional supervisions, i.e., APS and ACS.

We briefly describe *DNet* and *Confnet* whose architecture design is not the main focus of this work, and we discard the subscripts for a general description since the two branches share the identical architecture (but with a different weight initialization).

2) *Disparity Estimation Network (DNet)*: *DNet* first utilizes a weight-sharing ResNet-like network to extract features from I_l and I_r , yielding two downscaled feature maps F_l and F_r with the size of $320 \times H/4 \times W/4$. Like GwcNet [21], F_l and F_r are fused to construct a feature volume C_{feat} with the size of $64 \times H/4 \times W/4 \times S/4$. The last dimension of C_{feat} defines a disparity searching space (also downscaled) with a disparity range from 0 to $S - 1$ pixels.

Next, a 3D Attention CNN is used to aggregate and regularize C_{feat} into a cost volume C (CV) with the size of $H \times W \times S$. The 3D Attention CNN consists of three cascaded U-Nets [22]. In each U-Net, the channel attention mechanism is embedded after the last encoding layer to enhance interdependency of features at different disparity levels. After that, a softmax function [23] converts C to a map of disparity probability distribution P , which is calculated as follows:

$$P(x, y, s) = \frac{\exp(-C(x, y, s))}{\sum_{s=0}^{S-1} \exp(-C(x, y, s))} \quad (1)$$

where $s = 0, 1, \dots, S - 1$. $P(x, y, s)$ indicates a probability of the disparity being s pixels at the position (x, y) .

Finally, a map of disparity value D is calculated as the expectation of P , which is formulated in Eq. (2).

$$D(x, y) = \sum_{s=0}^{S-1} s \times P(x, y, s) \quad (2)$$

3) *Confidence Network (Confnet)*: *Confnet* follows *DNet*, and estimates how accurate the prediction of *DNet* is. *Confnet* takes the predicted CV as an input, and utilizes two convolutional layers and a batch normalization to generate

a confidence map K , whose values are normalized via a sigmoid into a range from 0 to 1. Lower values in K indicate higher possibilities that errors occur on the corresponding spatial positions in D .

B. Self-supervised Learning via APS and ACS

1) *Adaptive Parallel Supervision (APS)*: As shown in the bottom-left part of Figure 2 where the knowledge flows from Branch A to Branch B, APS treats D_a from Branch A as a pseudo ground-truth (GT) value map, denoted as $\hat{D}_{b|self}$, to guide the learning of Branch B by minimizing the smooth L1 loss (see Eq. (3)) between $\hat{D}_{b|self}$ and D_b .

$$\text{smooth}_{L_1}(x) = \begin{cases} 0.5x^2, & \text{if } |x| < 1 \\ |x| - 0.5, & \text{otherwise} \end{cases} \quad (3)$$

To increase the reliability of $\hat{D}_{b|self}$, K_a is utilized in a re-weighting strategy to suppress the possible wrong predictions in $\hat{D}_{b|self}$.

On the opposite direction from Branch B to Branch A, APS also minimizes the smooth L1 loss by treating D_b as a pseudo GT value map, denoted as $\hat{D}_{a|self}$, to guide the learning of Branch A, and meanwhile utilizes K_b to suppress the unreliable predictions in $\hat{D}_{a|self}$.

Thus, the final bidirectional APS loss \mathcal{L}_{APS} considers both parallel directions of knowledge flow between the two branches, and is formulated as follows:

$$\mathcal{L}_{APS} = \frac{1}{HW} \sum_{x,y} \left\{ \underbrace{K_a(x, y) \cdot \text{smooth}_{L_1}(D_b(x, y) - \hat{D}_{b|self}(x, y))}_{A \rightarrow B} + \underbrace{K_b(x, y) \cdot \text{smooth}_{L_1}(D_a(x, y) - \hat{D}_{a|self}(x, y))}_{B \rightarrow A} \right\} \quad (4)$$

where $\hat{D}_{b|self} = D_a$, $\hat{D}_{a|self} = D_b$.

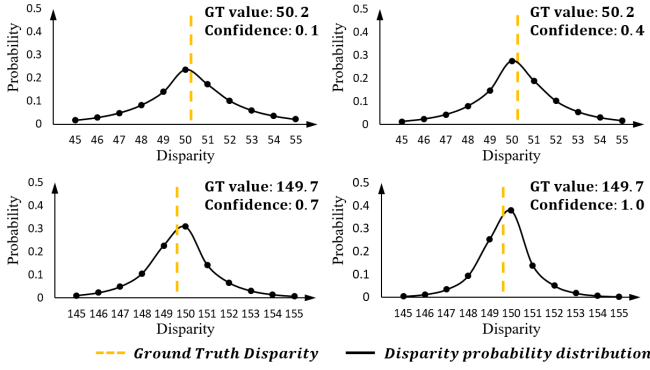


Fig. 3. Four examples of unimodal disparity probability distribution generated by our designed non-parametric operation of unimodal generation. After the operation, the disparity values can be softened into distributions, where the peak aligns the GT value, and is wider and lower if the confidence decreases.

It is worth noting that the gradients derived from minimizing the first and second item in Eq. (4) only update the weights of $DENet_b$ and $DENet_a$, respectively.

2) Adaptive Cross Supervision (ACS): If we only constrain the disparity value, there could be an abnormal solution where an erroneous distribution happens to derive a correct disparity value, therefore, the network learns questionable feature relations at some disparity levels. To avoid this, we additionally constrain the predicted distribution map in ACS.

As shown in the bottom-right part of Figure 2 where the knowledge flows from *Branch A to Branch B*, ACS constructs a pseudo GT distribution map $\hat{P}_{b|self}$ from $\hat{D}_{b|self}$ to supervise the learning of Branch B. To this end, we create three rules to the construction procedure of GT distribution:

- (1) The constructed GT disparity probability distribution obeys a unimodal distribution;
- (2) The peak of the unimodal distribution locates around the corresponding true disparity value;
- (3) The peak distribution is wider if the disparity value is more difficult to estimate (lower prediction confidence).

The first two rules are motivated by a fact that the disparity probability distribution actually reflects how well a pixel pair matches each other at different disparity levels. Therefore, the matching degree should reach its maximum around the true disparity, and decreases as the disparity level gets away from the true value. The third rule is inspired by the label-softening technique [24] which is widely employed in the classification task. A hard classification label is better to be softened from a one-hot vector to a distribution if this particular class is easily confused with others. In our case, we smooth the GT unimodal distribution of the regions with low confidence where the true disparity could be easily confused with its nearby values.

To obey the above three rules, we design a non-parametric operation of unimodal generation (denoted as UG), which inputs the GT value and confidence, and outputs a corresponding GT distribution. Therefore, we have $\hat{P}_{b|self} = UG(\hat{D}_{b|self}, K_b)$, and $\hat{P}_{b|self}(x, y, s)$ is calculated as follows:

$$\hat{P}_{b|self}(x, y, s) = \frac{\exp(-|s - \hat{D}_{b|self}(x, y)| \cdot \rho_b(x, y))}{\sum_{s=0}^{S-1} \exp(-|s - \hat{D}_{b|self}(x, y)| \cdot \rho_b(x, y))} \quad (5)$$

where $\hat{D}_{b|self} = D_a$.

According to Eq. (5), $\hat{P}_{b|self}(x, y, s)$ reaches its maximum if s is closest to $\hat{D}_{b|self}(x, y)$, and decreases otherwise, which obeys the first and second rules. $\rho_b(x, y)$ controls the smoothness of $\hat{P}_{b|self}$, and is calculated as follows:

$$\rho_b(x, y) = \frac{1}{2 - K_b(x, y)} \quad (6)$$

According to Eq. (6), $\rho_b(x, y)$ ranges from 0.5 to 1.0, and is positively correlated to the prediction confidence $K_b(x, y)$. If $K_b(x, y)$ decreases (confidence gets lower), $\rho_b(x, y)$ decreases accordingly, and narrows the gap of the power values of Euler's number e in Eq. (5). Consequently, the resulting distribution becomes wider, which obeys the third rule. Figure 3 presents four disparity probability distributions generated from different GT and confidence values.

On the opposite direction from *Branch B to Branch A*, ACS also constrains the probability distribution by constructing $\hat{P}_{a|self} = UG(\hat{D}_{a|self}, K_a)$ to guide the learning of Branch A, where $\hat{D}_{a|self} = D_b$.

Thus, the final bidirectional ACS loss \mathcal{L}_{ACS} considers both cross directions of knowledge flow between the two branches, and is formulated as follows:

$$\mathcal{L}_{ACS} = -\frac{1}{HW} \sum_{x,y} \sum_{s=0}^{S-1} \left\{ \underbrace{\hat{P}_{b|self}(x, y, s) \cdot \log P_b(x, y, s)}_{A \rightarrow B} + \underbrace{\hat{P}_{a|self}(x, y, s) \cdot \log P_a(x, y, s)}_{B \rightarrow A} \right\} \quad (7)$$

Similar to APS, the first and second items in Eq. (7) are minimized to update $DENet_b$ and $DENet_a$, respectively.

The total self-supervised loss to optimize the dual-branch network can be formulated as follows:

$$\mathcal{L}_{self} = \mathcal{L}_{APS} + \mathcal{L}_{ACS} \quad (8)$$

C. Fully-Supervised Learning of Each Branch

As an example in Branch A (the same in Branch B), Figure 4 details the fully-supervised learning of each branch on a labeled sample with its GT disparity map \hat{D} provided. We employ three losses for containing the predicted confidence $K_a(K_b)$, disparity value $D_a(D_b)$ and disparity probability distribution $P_a(P_b)$. Note that, our previous work [5] only optimized the losses for confidence and disparity value, which actually trained $DENet$ and $Confnet$ separately. In this work, we introduce an auxiliary loss for disparity probability distribution, optimizing which forces $DENet$ and $Confnet$ to be trained jointly.

1) Confidence Constraint: We treat the confidence estimation as a binary classification task, and thus define a positive class of high confidence as the prediction whose error is within 3 pixels, or a negative class of low confidence otherwise.

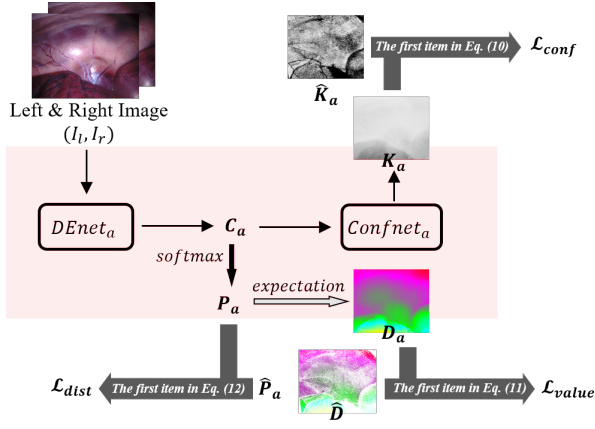


Fig. 4. Illustration of the fully-supervised learning of each branch (Branch A as an example). \mathcal{L}_{value} is minimized for updating $DNet$ only, \mathcal{L}_{conf} is minimized for updating $Confnet$ only, and \mathcal{L}_{dist} is minimized for updating $DNet$ and $Confnet$ jointly.

Therefore, the GT confidence map \hat{K}_a for Branch A can be generated as follows:

$$\hat{K}_a(x, y) = \begin{cases} 1, & \text{if } |D_a(x, y) - \hat{D}(x, y)| < 3 \\ 0, & \text{otherwise} \end{cases} \quad (9)$$

Likewise, we can also generate the GT confidence map \hat{K}_b for Branch B. The loss \mathcal{L}_{conf} based on Binary Cross Entropy loss is used to train the two confidence networks in both branches:

$$\begin{aligned} \mathcal{L}_{conf} = & -\frac{1}{HW} \sum_{x,y} \{ \hat{K}_a(x, y) \cdot \log K_a(x, y) + (1 - \hat{K}_a(x, y)) \cdot \log(1 - K_a(x, y)) \\ & + \hat{K}_b(x, y) \cdot \log K_b(x, y) + (1 - \hat{K}_b(x, y)) \cdot \log(1 - K_b(x, y)) \} \end{aligned} \quad (10)$$

2) Disparity Value Constraint: We calculate the smooth L1 loss (see Eq. (3)) between the predicted and GT disparity value map \hat{D} to train the two disparity estimation networks in both branches. In addition, we use a weight related to the GT disparity value to address the potential long-tail problem. Therefore, the loss \mathcal{L}_{value} based on the disparity-aware smooth L1 loss is formulated in Eq. (11).

$$\begin{aligned} \mathcal{L}_{value} = & \frac{1}{HW} \sum_{x,y} \alpha(x, y) \cdot \{ smooth_{L1}(D_a(x, y) - \hat{D}(x, y)) \\ & + smooth_{L1}(D_b(x, y) - \hat{D}(x, y)) \} \end{aligned} \quad (11)$$

where $\alpha(x, y) = \hat{D}(x, y) / \max(\hat{D})$ is defined as the normalized disparity.

3) Disparity Probability Distribution Constraint: Similar to ACS described in Sec. II-B, we also constrain the predicted probability distribution on each labeled sample to avoid the erroneous predictions. To this end, we utilize the unimodal generator to convert \hat{D} into two GT maps of disparity probability distribution for the two branches, that is, $\hat{P}_a = UG(\hat{D}, K_a)$, $\hat{P}_b = UG(\hat{D}, K_b)$.

Therefore, the loss \mathcal{L}_{dist} for constraining the predicted distributions is calculated as follows:

$$\begin{aligned} \mathcal{L}_{dist} = & -\frac{1}{HW} \sum_{x,y} \sum_{s=0}^{S-1} \{ \hat{P}_a(x, y, s) \cdot \log P_a(x, y, s) \\ & + \hat{P}_b(x, y, s) \cdot \log P_b(x, y, s) \} \end{aligned} \quad (12)$$

The fully-supervised loss \mathcal{L}_{full} is finally formulated in Eq. (13).

$$\mathcal{L}_{full} = \lambda_{conf} \mathcal{L}_{conf} + \mathcal{L}_{value} + \mathcal{L}_{dist} \quad (13)$$

where λ_{conf} denotes a weight coefficient, and is tuned to 8 in our experiments.

D. Implementation and Training Details

Our model was developed using PyTorch and trained on a single NVIDIA GeForce Titan-RTX GPU. We pre-trained a $DNet$ on Sceneflow dataset for 10 epochs, and utilized it as $DNet_a$ and $DNet_b$, except that the weights of the last two layers are initialized differently based on two random seeds. All weights of $Confnet_a$ and $Confnet_b$ were initialized differently.

We adopted an Adam optimizer ($\beta_1=0.9$, $\beta_2=0.999$) [25] to train our model. \mathcal{L}_{self} and \mathcal{L}_{full} are calculated using the unlabeled and labeled samples, respectively. The gradients derived from minimizing \mathcal{L}_{full} update the weights of both disparity estimation and confidence networks, and those from minimizing \mathcal{L}_{self} only update the disparity estimation networks. The losses on the reflective regions were masked out, and the reflective pixels were classified if their saturation value is less than 0.1 and intensity value is greater than 0.9.

The total number of training epochs varied according to different datasets, and is detailed in Sec. IV. The initial learning rate was set to 0.001 and halved after every quarter of the total epoch number. In the training phase, we randomly cropped image patch pairs with size of 256×256 , and each patch pair was augmented by a random horizontal flip, gamma and brightness shifts. We set the disparity searching range to $[0, 192]$ in the calculation of cost volume.

III. EXPERIMENTAL SETTINGS

A. State-of-the-arts methods

We compare our method with several state-of-the-art methods including two traditional algorithms, four fully-supervised and four semi-supervised methods.

The traditional algorithms for comparison are SGM [26] and Stereo-UCL [27], which are available in the OpenCV toolbox. In our experiments, SGM gets its best performance by setting aggregation paths $Dir = 8$, smoothness penalties $P1 = 7$ and $P2 = 100$. Stereo-UCL has no parameters to tune.

The fully-supervised methods for comparison include GANet [4], PSMNet [28], HSMNet [29] and CFNet [30]. These methods are open source, and we use their released models for fine-tuning according to their recommended parameters. The semi-supervised methods for comparison include Smolyanskiy et al. [18], Ji et al. [31], Soft MT [32] and Improved TSN [5]. The methods [18], [31] were originally proposed for depth estimation. We re-implement these two methods following their papers due to the lack of released

source codes. Soft MT [32] is a competitive semi-supervised method for object detection. We compare with Soft MT since it belongs to the family of TSN like ours and released its source code. In Soft MT, the knowledge flow between the teacher and student models is still unidirectional, but the two models are trained synchronously in an exponential mean average (EMA) manner. Improved TSN [5] is our previous work.

Note that, we replace the backbone with our employed *DEnet* in the two methods [31], [32], because their developed backbones are for the task of monocular depth estimation and object detection respectively, and thus incompatible with the task we focus on in this paper.

B. Datasets

This study includes three public datasets, i.e., SCARED [9], SERV-CT [33] and KITTI 2012 [34].

1) **SCARED**: SCARED is one of the MICCAI 2019 challenges [9], and provided a training set acquired from 7 pigs. Each pig corresponds to 5 videos recorded by a binocular camera from 5 different views of the abdominal anatomy scene. The video resolution is 1024×1280 , and the first frame of each video was marked as a keyframe. The ground-truth (GT) depth maps of keyframes were obtained by structured light projection directly, and those of the following video frames were approximated indirectly by depth interpolation using the transformation matrix relative to the keyframe camera position. Details about this dataset can be found in [9].

There are two inaccuracies in the training set [9]. First, the 4th and 5th subjects have to be excluded for calibration parameter errors. Second, except keyframes, the video frames and GT depth maps are misaligned temporally. Thus, we only use the keyframes of the rest 5 pigs and their corresponding GT depth maps in our experiments. This leaves us $5 \times 5 = 25$ labeled keyframes in total for evaluation. In addition, we extract 250 frames from each subject as unlabeled samples.

Recently, the challenge also released the official test set acquired from two extra pigs. Likewise, each pig corresponds to 5 binocular videos, and the first frame of each video was marked as a keyframe. Note that, the 5th video of each pig only contains a single frame, that is, the video is identical to the keyframe. The GT depth maps of all frames were also released.

2) **SERV-CT**: The SERV-CT dataset was collected from 2 *ex-vivo* porcine cadavers abdomen and each pig corresponds to 8 binocular image pairs with the size of 576×720 . Both GT depth and disparity maps were provided.

3) **KITTI 2012**: KITTI 2012 is a real-world dataset in the outdoor scenario, and contains 194 stereo image pairs with the size of 376×1240 , and their corresponding GT disparity maps captured by LiDAR.

C. Evaluation Metrics

For SCARED, we use the provided stereo calibration parameters to convert the GT depth into the GT disparity maps. The evaluation metrics are disparity mean absolute error (MAE) and percentages of 1-px, 2-px, 3-px disparity outliers. Outliers are defined as the pixels whose disparity error is greater than a threshold (i.e., one, two or three pixels). On the two extra

test subjects of SCARED, we also use the official metric, i.e., depth MAE, for evaluation.

For SERV-CT, the evaluation metrics are percentage of 3-px disparity outliers and root mean square error (RMSE) for depth and disparity. For KITTI, we utilize the evaluation metric of disparity MAE. The calculation of MAE and RMSE is formulated in Eq. (14) and Eq. (15).

$$MAE = \frac{1}{N} \sum_{x,y} |D(x,y) - \hat{D}(x,y)| \quad (14)$$

$$RMSE = \sqrt{\frac{1}{N} \sum_{x,y} (D(x,y) - \hat{D}(x,y))^2} \quad (15)$$

where N represents the total number of labeled pixels.

IV. RESULTS AND DISCUSSIONS

A. Comparison with State-of-the-arts

1) **Evaluation on SCARED (5-fold cross-validation)**: We conduct a 5-fold cross-validation on SCARED, that is, 20 labeled keyframes plus 1000 unlabeled video frames for training and 5 keyframes for test in each round of cross-validation. No subject is cross-used in the training and test folds. The total number of training epochs is set to 100. Table I lists the comparison results between our method and the state-of-the-art methods. A lower value in this table indicates a better performance for all metrics. Note that, the two branches of our method predict independently in the reference phase, and we only report the prediction whose confidence map has the larger average value.

From Table I, we can have three key observations:

(i) The performance of the two traditional methods is similar, but both relatively unsatisfying compared to that of the learning-based methods, demonstrating a powerful reasoning capability of CNNs;

(ii) The performance of the fully-supervised methods (3rd to 6th rows) is mostly lower than that of the semi-supervised methods (7th to 11th rows), because the latter utilized unlabeled samples to avoid the overfitting problem;

(iii) Our method achieves a superior performance by decreasing disparity MAE by **13.95%** compared to the fully-supervised model CFNet ($p < 0.001$), and by **9.76%** comparing to the semi-supervised model Soft MT ($p < 0.001$). Compared to the second best method Improved TSN, our method reduces disparity MAE by **3.90%** ($p = 0.002$), which mainly benefits from two ameliorations, that is, the two learners in our method mutually guide each other in an adaptive bidirectional learning, and *Confnet* and *DEnet* are trained jointly by the constraint of disparity probability distribution.

Figure 5 visualizes the results of different methods, i.e., the two best fully-supervised methods, the two best semi-supervised methods and ours. The error map is obtained by calculating the absolute distance between the GT and predicted disparity for every position. As can be seen, the semi-supervised methods are better than the fully-supervised methods, and our method achieves the most accurate disparity prediction among them (see the red arrows), especially at the flat areas (the 1st and 2nd rows) or the organ edges (the 3rd row).

TABLE I

COMPARISON RESULTS OF 5-FOLD CROSS-VALIDATION ON SCARED. THE BEST PERFORMANCE IS MARKED IN BOLD. * INDICATES THAT THE P-VALUES OF OUR METHOD ARE ALL LESS THAN 0.05 WHEN COMPARING TO OTHER METHODS.

Methods	Supervision	>1px (%)	>2px (%)	>3px (%)	Disparity MAE (px)
SGM [26]	-	30.04 ± 11.52	8.67 ± 6.22	3.71 ± 3.13	1.25 ± 0.14
Stereo-UCL [27]	-	32.98 ± 7.90	10.93 ± 5.47	4.72 ± 3.04	1.21 ± 0.21
GANet [4]	Fully	25.36 ± 11.16	7.04 ± 4.97	2.96 ± 2.46	1.01 ± 0.20
PSMNet [28]	Fully	26.53 ± 10.16	7.25 ± 4.91	2.88 ± 2.46	0.92 ± 0.12
HSMNet [29]	Fully	25.11 ± 9.71	6.56 ± 4.56	2.57 ± 2.42	0.88 ± 0.12
CFNet [30]	Fully	23.60 ± 10.80	6.19 ± 4.68	2.48 ± 2.46	0.86 ± 0.13
Smolyanskiy et al. [18]	Semi	24.10 ± 10.71	6.55 ± 4.90	2.72 ± 2.66	0.86 ± 0.14
Ji et al. [31]	Semi	23.65 ± 9.95	6.00 ± 4.38	2.39 ± 2.29	0.84 ± 0.12
Soft MT [32]	Semi	23.11 ± 9.99	5.81 ± 4.17	2.25 ± 2.26	0.82 ± 0.11
Improved TSN [5]	Semi	22.32 ± 9.66	5.51 ± 3.72	2.04 ± 1.87	0.77 ± 0.11
Ours	Semi	20.31 ± 9.83*	5.01 ± 3.87*	1.96 ± 1.88	0.74 ± 0.11*

TABLE II

THE CHALLENGE LEADERBOARD OF SCARED ON TWO TEST SUBJECTS. KN IS DEPTH MAE ON THE N-TH KEYFRAME OF EACH SUBJECT. AVG. IS AVERAGE DEPTH MAE ON ALL VIDEO FRAMES. THE BEST PERFORMANCE IS MARKED IN BOLD, AND THE SECONDARY BEST PERFORMANCE IS MARKED WITH UNDERLINE.

Methods	The 1st test subject						The 2nd test subject					
	k1	k2	k3	k4	k5	Avg.	k1	k2	k3	k4	k5	Avg.
J.C. Rosenthal	8.25	3.36	2.21	2.03	1.33	3.44	8.26	2.29	7.04	2.22	0.42	4.05
Trevor Zeffiro	7.91	2.97	<u>1.71</u>	2.52	2.91	3.60	5.39	1.67	4.34	3.18	2.79	3.47
Dimitris Psychogyios 1	7.73	<u>2.07</u>	1.94	2.63	<u>0.62</u>	3.00	4.85	1.23	3.52	1.95	<u>0.41</u>	2.39
Dimitris Psychogyios 2	7.41	2.03	1.92	2.75	0.65	<u>2.95</u>	4.78	1.19	<u>3.34</u>	1.82	0.36	2.30
Sebatian Schmid	<u>7.61</u>	2.41	1.84	2.48	0.99	<u>3.07</u>	<u>4.33</u>	<u>1.10</u>	<u>3.65</u>	<u>1.69</u>	<u>0.48</u>	<u>2.25</u>
Ours	7.98	2.24	1.67	2.02	0.54	2.89	4.28	1.04	3.30	1.68	<u>0.41</u>	2.14

TABLE III

LEAVE-ONE-OUT EVALUATION RESULTS ON SERV-CT. THE BEST PERFORMANCE IS MARKED IN BOLD.

Methods	Supervision	> 3px (%)		Depth RMSE (mm)		Disparity RMSE (px)	
		Noc	All	Noc	All	Noc	All
HSMNet [29]	Fully	5.63	8.52	2.13	2.93	1.59	2.18
CFNet [30]	Fully	5.38	7.73	2.14	2.97	1.50	2.20
Soft MT [32]	Semi	5.08	8.01	2.12	2.96	1.46	2.19
Improved TSN [5]	Semi	4.29	6.96	2.24	2.89	1.51	2.10
Ours	Semi	3.99	6.32	1.99	2.72	1.34	1.86

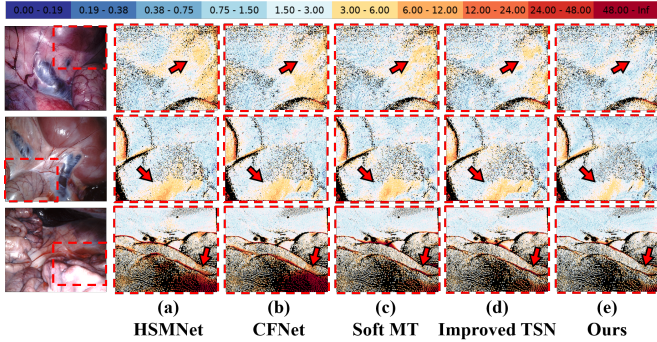


Fig. 5. Error map of predicted disparities on three SCARED samples. The left-most col shows the input left images. (a)-(e) are results of the two best fully-supervised methods, the two best semi-supervised methods and our method. Different colors indicate different absolute distances between the GT and predicted disparity.

2) *Evaluation on SCARED (challenge leaderboard)*: We use the labeled keyframes and unlabeled video frames of all 5 training subjects to re-train our model, and perform evaluation on the two official test subjects. Following the recommended evaluation protocol in [9], the evaluation is performed on all video frames except in which whose more than 90% of GT maps is empty. For each test subject, the depth MAE on

each keyframe and the average depth MAE of all frames are reported. Table II lists the comparison results between our method and other challenge participants whose results were reported in [9].

The first two rows of Table II are the runner-up and winner of the challenge. After the challenge, the organizers allowed a period of late submission, and the three teams (the 3rd to 5th rows) were added into the leaderboard. As the official challenge winner, Trevor Zeffiro achieves an average depth MAE of 3.60 mm and 3.47 mm on the two test subjects, respectively. In comparison, our method reduces the average depth MAE by **19.72%** and **38.3%**.

Among the late submissions, two teams achieve impressive results. Dimitris Psychogyios 2 finetuned HSMNet [29] model on SCARED and achieves an average depth MAE of 2.95 mm and 2.30 mm. Sebatian Schmid used a 3D CV based method for stereo matching and achieves an average depth MAE of 3.07 mm and 2.25 mm. Compared to these two teams, our method reduces the average depth MAE to 2.89 mm and 2.14 mm, which surpasses Dimitris Psychogyios 2 by **2.03%** and **6.96%**, and Sebatian Schmid by **5.86%** and **4.89%** on two test subjects.

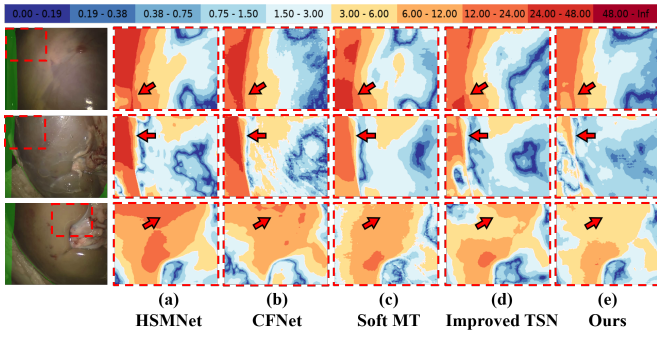


Fig. 6. Error map of predicted disparities on three SERV-CT samples. The left-most col shows the input left images where the green transparent regions are occluded in the right counterpart. (a)-(e) are results of the two best fully-supervised methods, the two best semi-supervised methods and our method. Different colors indicate different absolute distances between the GT and predicted disparity.

3) *Evaluation on SERV-CT*: We compare our method with the two best fully-supervised methods HSMNet and CFNet, and the two best semi-supervised methods Soft MT and Improved TSN, on SERV-CT. We conduct a leave-one-out evaluation. In each round, we additionally include the labeled and unlabeled samples from SCARED to enlarge the training data size. The total number of training epochs is set to 100.

Table III lists the comparison results for both non-occluded (Noc) and all (All) pixels. From these results, three conclusions can be made:

(i) The performance of Soft MT is only comparable to that of the two fully-supervised methods. Therefore, the semi-supervised learning should not be overused for unlabeled images from a different data source;

(ii) Improved TSN successfully draws useful knowledge from the unlabeled samples, and thus surpasses Soft MT and the two fully-supervised methods in terms of most metrics. Therefore, error suppression on pseudo labels is of great importance when unlabeled data from other source are used;

(iii) Our method achieves a superior performance in terms of all metrics, and reduces disparity RMSE by at least **8.22%** and **11.43%** on non-occluded pixels and all pixels, respectively.

Figure 6 visualizes error maps of the comparison methods. The error maps of Improved TSN and ours are bluer in the occluded areas, which demonstrates the importance of error suppression of pseudo labels. There are less red and no dark-red regions in our error maps, especially on the flat and low-textured organ surfaces (see the red arrows).

B. Ablation Studies

We conduct several ablation studies to verify the effectiveness of the two adaptive bidirectional supervisions, APS and ACS, and the joint learning of *DEnet* and *Confnet*. SCARED and 5-fold cross validation are adopted.

1) *Effectiveness of APS and ACS*: We train four variants of our dual-branch CNN by using APS and/or ACS and none of both. The model that is w/o both is treated as baseline, and identical to a single branch trained on only labeled samples. The other three models are trained on both labeled and unlabeled samples. The comparison results of the four variants are listed in Table IV. The statistical test is also performed on

TABLE IV

COMPARISON RESULTS OF FOUR VARIANTS OF OUR METHOD. THE BEST PERFORMANCE IS MARKED IN BOLD.

Variant Models	>3px (%)	Disparity MAE (px)
w/o Both (Baseline)	2.44 ± 2.33	0.84 ± 0.10
w/ APS only	2.20 ± 2.16	0.80 ± 0.10
w/ ACS only	2.09 ± 2.20	0.78 ± 0.11
w/ Both (Complete)	1.96 ± 1.88	0.74 ± 0.11

TABLE V

COMPARISON RESULTS BETWEEN TWO VARIANTS USING STATIC OR ADAPTIVE SUPERVISIONS. SCU MEANS THE SUM OF AVERAGE CONFIDENCE OF UNLABELED SAMPLES.

Supervision	SCU	>3px (%)	Disparity MAE (px)
Static	903.6	2.14 ± 2.22	0.78 ± 0.11
Adaptive	968.7	1.96 ± 1.88	0.74 ± 0.11
		p-values	
Adaptive vs. Static		0.0424	0.0001

pairwise comparison of every two variants. We used paired-samples T-test which is implemented in the SPSS software for statistical test.

Either APS or ACS can obtain a performance gain compared to baseline ($p = 0.005$, $p = 0.015$ in terms of Disparity MAE), but using ACS is more effective than using APS by reducing disparity MAE by 7.14% ($p = 0.06$). Also, APS and ACS are not mutually excluded, and together can further reduce disparity MAE by 6.33% and 5.06% ($p = 0.002$, $p < 0.001$), compared to APS only and ACS only, respectively.

It is worth noting that the model before using APS and ACS is inferior to the two TSN-based methods Soft MT and Improved TSN (Table I), but becomes superior to all compared state-of-the-arts after being equipped with the adaptive bidirectional supervisions.

2) *Adaptive vs. Static supervisions*: We train two variants of our dual-branch CNN. One is the complete version using adaptive supervisions where potential errors are suppressed and labels of hard samples are softened, and the other uses static supervisions where no pseudo supervision is suppressed and ρ in Eq. (6) is constant one.

The comparison results of the two variants are listed in Table V. The adaptively-supervised model expectedly achieves a promising improvement in terms of all metrics ($p < 0.05$), compared to those using static supervisions. This well verifies the significant role of *Confnet* in our dual-branch CNN for the semi-supervised learning.

We also calculate the sum of average confidence of unlabeled samples (SCU). An increase of SCU indicates that more predictions can be effectively utilized as pseudo supervisions, reflecting a higher efficacy of unlabeled samples in the self-supervised training. From the 2nd column of Table V, the model with adaptive supervisions has a higher quality of pseudo supervisions, with around 65 more unlabeled samples usable for training.

3) *Bidirectional vs. Unidirectional supervisions*: We compare the model with bidirectional supervision to that with unidirectional to verify the importance of the mutual guidance in the self-supervised learning. The comparison results are listed

TABLE VI

COMPARISON RESULTS BETWEEN TWO VARIANTS WHOSE SELF-SUPERVISIONS ARE BIDIRECTIONAL OR UNIDIRECTIONAL. SCU MEANS THE SUM OF AVERAGE CONFIDENCE OF UNLABELED SAMPLES.

Supervision	SCU	>3px (%)	Disparity MAE (px)
Unidirectional	862.5	2.34 ± 2.30	0.81 ± 0.10
Bidirectional	968.7	1.96 ± 1.88	0.74 ± 0.11
p-values			
Bidirc. vs. Unidirc.		0.0027	0.0008

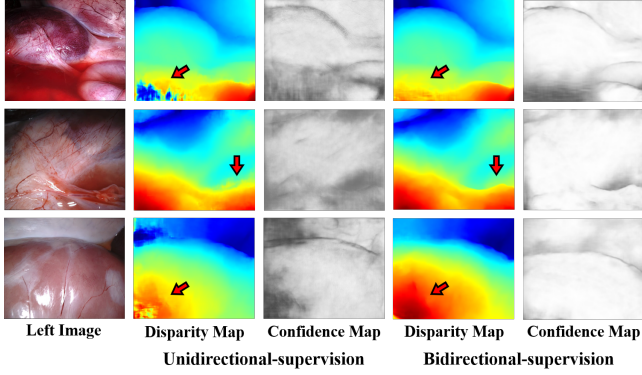


Fig. 7. Three examples of the predicted disparity and confidence maps by the two variants of our method. Darker areas in the confidence map have lower confidence.

in Table VI. The bidirectional knowledge flow can make the two branches eventually converge on more accurate disparity estimation by reducing Disparity MAE by 8.64% compared to that with the unidirectional knowledge flow ($p < 0.001$). Also, SCU increases from 862.5 to 968.7 as the two branches are enabled to teach each other.

Figure 7 further visualizes the disparity maps and confidence maps of unlabeled samples predicted by the comparison models. *Confnet* of both models successfully classifies the regions with possible errors as low confidence. Overall, the confidence maps predicted under bidirectional supervisions are brighter (higher confidence) than those under unidirectional supervisions (the 3rd vs. 5th column). Therefore, more unlabeled samples with high confidence can be utilized to improve the model performance, which is also evidenced by the increase of SCU in Table VI. As indicated by the black dotted boxes in Figure 7, the model trained under bidirectional supervisions predicts more reasonable disparities on the challenging regions, such as blood (the 1st row), edge (the 2nd row) and reflective surface (the 3rd row), than that trained under unidirectional (see the red arrows).

4) *Joint vs. Separate learning*: We verify the performance gain by additionally introducing the distribution constraint \mathcal{L}_{dist} in the fully-supervised learning. Therefore, we compare two variants of single-branch model with and without optimizing the disparity distribution constraint. *DEnet* and *Confnet* are trained jointly if using the constraint, and are trained separately otherwise.

The comparison results are listed in Table VII. Joint training achieves a significant improvement in terms of both metrics ($p < 0.05$). We believe the reason is that the confidence from *Confnet* plays a role of softening labels of hard samples to

TABLE VII

COMPARISON RESULTS BETWEEN TWO VARIANTS OF THE SINGLE-BRANCH CNN WHOSE *DEnet* and *Confnet* ARE TRAINED JOINTLY OR SEPARATELY.

Learning	>3px (%)	Disparity MAE (px)
Separate	2.58 ± 2.34	0.87 ± 0.11
Joint	2.44 ± 2.33	0.84 ± 0.10
p-values		
Joint vs. Separate	0.0452	0.0060

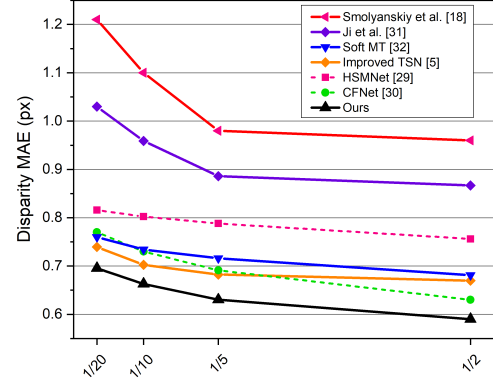


Fig. 8. Performance curves on KITTI of different methods which are trained under different proportions of available labels.

enhance the learning of *DEnet* effectively.

C. Learning Efficiency of Semi-supervised Methods

We use the KITTI 2012 dataset to evaluate training efficiency. To this end, we split the dataset into 180 pairs for training and 14 for test, and train each semi-supervised method four times. In each time, we randomly selected a small proportion of training samples as labeled ones (i.e., 5%, 10%, 20%, and 50%, respectively), and the rest as unlabeled ones, and the total number of training epochs is set to 600.

Figure 8 illustrates the performance trajectory in terms of Disparity MAE at different label proportions of the semi-supervised methods, i.e., Smolyanskiy et al. [18], Ji et al. [31], Soft MT [32] and Improved TSN [5], and our method. The curves of Soft MT, Improved TSN and ours are lower than others' by a large margin. Moreover, our method consistently surpasses others regardless of the number of labels used for training. Especially, our method with only 1/20 labels achieves a comparable performance to Soft MT and Improved TSN with 1/5 or even 1/2 labels.

We also compare with the two best fully-supervised methods, i.e., HSMNet [29] and CFNet [30] (see the two dashed lines). When the proportion of labeled samples is less than 1/5, Improved TSN and our method are better than the two fully-supervised methods. As the number of labels further increases, Improved TSN is inferior to CFNet, while our method is still the best.

V. CONCLUSION

In this paper, we successfully addressed the stagnant quality of pseudo labels caused by the teacher-to-student unidirectional knowledge flow in our previous work Improved TSN

[5]. Specifically, we proposed a novel dual-branch CNN with two kinds of adaptive bidirectional supervisions, named APS and ACS, in a semi-supervised manner. With APS and ACS, the two branches can mutually guide each other by taking the opposite's predictions as pseudo supervisions. Differently, APS constrains the predicted disparity values, while ACS forces the predicted disparity probability distributions to be unimodal. This not only guarantees accurate disparity estimation, but also makes sure that the right disparity value is indeed from a correct distribution by learning reasonable feature matching relations in the left-right image pair. In addition, we introduced a confidence network in each branch to estimate the reliability of their predictions, and to adaptively refine pseudo supervisions flowing across branches. Finally, with the well-tuned bidirectional supervisions, we maximized the efficacy of unlabeled samples, and jointly optimized the two branches to converge on a consistent and more accurate disparity prediction.

We conducted extensive and comprehensive comparisons with the state-of-the-arts on three public datasets, i.e., SCARED, SERV-CT, KITTI. The comparison on SCARED demonstrated a superior performance of our method over other state-of-the-arts. The comparison on SERV-CT showed that the performance of our method can be more effectively enhanced by unlabeled samples from other data sources. The comparison on KITTI verified that our dual-branch CNN has a relatively higher efficiency of learning from unlabeled samples. Four ablation studies were also conducted, and well demonstrated the effectiveness of our proposed two kinds of adaptive bidirectional supervisions, i.e., ACS and APS, and the joint training of *DEnet* and *Confnet* by additionally constraining the disparity probability distribution.

REFERENCES

- [1] D. Stoyanov, G. P. Mylonas, M. Lerotic, A. J. Chung, and G.-Z. Yang, "Intra-operative visualizations: Perceptual fidelity and human factors," *Journal of Display Technology*, vol. 4, no. 4, pp. 491–501, 2008.
- [2] R. H. Taylor, A. Mencicassi, G. Fichtinger, P. Fiorini, and P. Dario, "Medical robotics and computer-integrated surgery," *Springer handbook of robotics*, pp. 1657–1684, 2016.
- [3] X. Mei, X. Sun, M. Zhou, S. Jiao, H. Wang, and X. Zhang, "On building an accurate stereo matching system on graphics hardware," in *2011 IEEE International Conference on Computer Vision Workshops (ICCV Workshops)*. IEEE, 2011, pp. 467–474.
- [4] F. Zhang, V. Prisacariu, R. Yang, and P. H. Torr, "Ga-net: Guided aggregation net for end-to-end stereo matching," in *Proceedings of the IEEE/CVF Conference on Computer Vision and Pattern Recognition*, 2019, pp. 185–194.
- [5] H. Shi, Z. Wang, J. Lv, Y. Wang, P. Zhang, F. Zhu, and Q. Li, "Semi-supervised learning via improved teacher-student network for robust 3d reconstruction of stereo endoscopic image," in *Proceedings of the 29th ACM International Conference on Multimedia*, 2021, pp. 4661–4669.
- [6] P.-L. Chang, D. Stoyanov, A. J. Davison *et al.*, "Real-time dense stereo reconstruction using convex optimisation with a cost-volume for image-guided robotic surgery," in *International Conference on Medical Image Computing and Computer-Assisted Intervention*. Springer, 2013, pp. 42–49.
- [7] V. Penza, J. Ortiz, L. S. Mattos, A. Forgione, and E. De Momi, "Dense soft tissue 3d reconstruction refined with super-pixel segmentation for robotic abdominal surgery," *International journal of computer assisted radiology and surgery*, vol. 11, no. 2, pp. 197–206, 2016.
- [8] A. Rau, P. Edwards, O. F. Ahmad, P. Riordan, M. Janatka, L. B. Lovat, and D. Stoyanov, "Implicit domain adaptation with conditional generative adversarial networks for depth prediction in endoscopy," *International journal of computer assisted radiology and surgery*, vol. 14, no. 7, pp. 1167–1176, 2019.
- [9] M. Allan, J. Mcleod, C. C. Wang, J. C. Rosenthal, K. X. Fu, T. Zeffiro, W. Xia, Z. Zhanshi, H. Luo, X. Zhang *et al.*, "Stereo correspondence and reconstruction of endoscopic data challenge," *arXiv preprint arXiv:2101.01133*, 2021.
- [10] F. Mahmood and N. J. Durr, "Deep learning and conditional random fields-based depth estimation and topographical reconstruction from conventional endoscopy," *Medical image analysis*, vol. 48, pp. 230–243, 2018.
- [11] H. Luo, Q. Hu, and F. Jia, "Details preserved unsupervised depth estimation by fusing traditional stereo knowledge from laparoscopic images," *Healthcare technology letters*, vol. 6, no. 6, p. 154, 2019.
- [12] W. Cui, Y. Liu, Y. Li, M. Guo, Y. Li, X. Li, T. Wang, X. Zeng, and C. Ye, "Semi-supervised brain lesion segmentation with an adapted mean teacher model," in *International Conference on Information Processing in Medical Imaging*. Springer, 2019, pp. 554–565.
- [13] X. Li, L. Yu, H. Chen, C.-W. Fu, and P.-A. Heng, "Semi-supervised skin lesion segmentation via transformation consistent self-ensembling model," *arXiv preprint arXiv:1808.03887*, 2018.
- [14] N. Mayer, E. Ilg, P. Hausser, P. Fischer, D. Cremers, A. Dosovitskiy, and T. Brox, "A large dataset to train convolutional networks for disparity, optical flow, and scene flow estimation," in *Proceedings of the IEEE conference on computer vision and pattern recognition*, 2016, pp. 4040–4048.
- [15] C. Godard, O. Mac Aodha, and G. J. Brostow, "Unsupervised monocular depth estimation with left-right consistency," in *Proceedings of the IEEE conference on computer vision and pattern recognition*, 2017, pp. 270–279.
- [16] M. Ye, E. Johns, A. Handa, L. Zhang, P. Pratt, and G.-Z. Yang, "Self-supervised siamese learning on stereo image pairs for depth estimation in robotic surgery," *arXiv preprint arXiv:1705.08260*, 2017.
- [17] B. Huang, J.-Q. Zheng, A. Nguyen, D. Tuch, K. Vyas, S. Giannarou, and D. S. Elson, "Self-supervised generative adversarial network for depth estimation in laparoscopic images," in *International Conference on Medical Image Computing and Computer-Assisted Intervention*. Springer, 2021, pp. 227–237.
- [18] N. Smolyanskiy, A. Kameney, and S. Birchfield, "On the importance of stereo for accurate depth estimation: An efficient semi-supervised deep neural network approach," in *Proceedings of the IEEE conference on computer vision and pattern recognition workshops*, 2018, pp. 1007–1015.
- [19] S. Laine and T. Aila, "Temporal ensembling for semi-supervised learning," *arXiv preprint arXiv:1610.02242*, 2016.
- [20] F. Tosi, F. Aleotti, M. Poggi, and S. Mattoccia, "Learning monocular depth estimation infusing traditional stereo knowledge," in *Proceedings of the IEEE/CVF Conference on Computer Vision and Pattern Recognition*, 2019, pp. 9799–9809.
- [21] X. Guo, K. Yang, W. Yang, and H. Li, "Group-wise correlation stereo network," in *Proceedings of the IEEE/CVF Conference on Computer Vision and Pattern Recognition*, 2019, pp. 3273–3282.
- [22] O. Ronneberger, P. Fischer, and T. Brox, "U-net: Convolutional networks for biomedical image segmentation," in *International Conference on Medical image computing and computer-assisted intervention*. Springer, 2015, pp. 234–241.
- [23] A. Kendall, H. Martirosyan, S. Dasgupta, P. Henry, R. Kennedy, A. Bachrach, and A. Bry, "End-to-end learning of geometry and context for deep stereo regression," in *Proceedings of the IEEE International Conference on Computer Vision*, 2017, pp. 66–75.
- [24] R. Müller, S. Kornblith, and G. E. Hinton, "When does label smoothing help?" *Advances in neural information processing systems*, vol. 32, 2019.
- [25] D. P. Kingma and J. Ba, "Adam: A method for stochastic optimization," *arXiv preprint arXiv:1412.6980*, 2014.
- [26] H. Hirschmüller, "Stereo processing by semiglobal matching and mutual information," *IEEE Transactions on pattern analysis and machine intelligence*, vol. 30, no. 2, pp. 328–341, 2007.
- [27] D. Stoyanov, M. V. Scarzanella, P. Pratt, and G.-Z. Yang, "Real-time stereo reconstruction in robotically assisted minimally invasive surgery," in *International Conference on Medical Image Computing and Computer-Assisted Intervention*. Springer, 2010, pp. 275–282.
- [28] J.-R. Chang and Y.-S. Chen, "Pyramid stereo matching network," in *Proceedings of the IEEE Conference on Computer Vision and Pattern Recognition*, 2018, pp. 5410–5418.
- [29] G. Yang, J. Manela, M. Hapold, and D. Ramanan, "Hierarchical deep stereo matching on high-resolution images," in *Proceedings of the IEEE/CVF Conference on Computer Vision and Pattern Recognition*, 2019, pp. 5515–5524.

- [30] Z. Shen, Y. Dai, and Z. Rao, "Cfnet: Cascade and fused cost volume for robust stereo matching," in *Proceedings of the IEEE/CVF Conference on Computer Vision and Pattern Recognition*, 2021, pp. 13 906–13 915.
- [31] R. Ji, K. Li, Y. Wang, X. Sun, F. Guo, X. Guo, Y. Wu, F. Huang, and J. Luo, "Semi-supervised adversarial monocular depth estimation," *IEEE transactions on pattern analysis and machine intelligence*, vol. 42, no. 10, pp. 2410–2422, 2019.
- [32] M. Xu, Z. Zhang, H. Hu, J. Wang, L. Wang, F. Wei, X. Bai, and Z. Liu, "End-to-end semi-supervised object detection with soft teacher," in *Proceedings of the IEEE/CVF International Conference on Computer Vision*, 2021, pp. 3060–3069.
- [33] P. E. Edwards, D. Psychogyios, S. Speidel, L. Maier-Hein, and D. Stoyanov, "Serv-ct: A disparity dataset from cone-beam ct for validation of endoscopic 3d reconstruction," *Medical image analysis*, vol. 76, p. 102302, 2022.
- [34] A. Geiger, P. Lenz, and R. Urtasun, "Are we ready for autonomous driving? the kitti vision benchmark suite," in *Conference on Computer Vision and Pattern Recognition (CVPR)*, 2012.